



LAWRENCE
LIVERMORE
NATIONAL
LABORATORY

Demonstration of a 17 cm robust carbon fiber deformable mirror for adaptive optics

S. M. Ammons, M. Hart, B. Coughenour, R. Romeo, R. Martin, M. Rademacher

September 14, 2011

SPIE Optics & Photonics
San Diego, CA, United States
August 21, 2011 through August 25, 2011

Disclaimer

This document was prepared as an account of work sponsored by an agency of the United States government. Neither the United States government nor Lawrence Livermore National Security, LLC, nor any of their employees makes any warranty, expressed or implied, or assumes any legal liability or responsibility for the accuracy, completeness, or usefulness of any information, apparatus, product, or process disclosed, or represents that its use would not infringe privately owned rights. Reference herein to any specific commercial product, process, or service by trade name, trademark, manufacturer, or otherwise does not necessarily constitute or imply its endorsement, recommendation, or favoring by the United States government or Lawrence Livermore National Security, LLC. The views and opinions of authors expressed herein do not necessarily state or reflect those of the United States government or Lawrence Livermore National Security, LLC, and shall not be used for advertising or product endorsement purposes.

Demonstration of a 17 cm robust carbon fiber deformable mirror for adaptive optics

S. Mark Ammons^{*a}, Michael Hart^b, Blake Coughenour^c, Robert Romeo^d, Robert Martin^d, Matt Rademacher^b

^aLawrence Fellow, Lawrence Livermore National Laboratory, Physics Division, L-210, 7000 East Ave., Livermore, CA USA 94550

^bSteward Observatory, University of Arizona, 933 Cherry Ave, Tucson, AZ USA 85721

^cCollege of Optical Sciences, University of Arizona, 1630 E. University Blvd., Tucson, AZ USA 85721

^dComposite Mirror Applications, 1638 Research Loop, Tucson, AZ, USA 85710

ABSTRACT

Carbon-fiber reinforced polymer (CFRP) composite is an attractive material for fabrication of optics due to its high stiffness-to-weight ratio, robustness, zero coefficient of thermal expansion (CTE), and the ability to replicate multiple optics from the same mandrel. We use 8 and 17 cm prototype CFRP thin-shell deformable mirrors to show that residual CTE variation may be addressed with mounted actuators for a variety of mirror sizes. We present measurements of surface quality at a range of temperatures characteristic of mountaintop observatories. For the 8 cm piece, the figure error of the Al-coated reflective surface under best actuator correction is ~ 43 nm RMS. The 8 cm mirror has a low surface error internal to the outer ring of actuators (17 nm RMS at 20°C and 33 nm RMS at -5°C). Surface roughness is low (< 3 nm P-V) at a variety of temperatures. We present new figure quality measurements of the larger 17 cm mirror, showing that the intra-actuator figure error internal to the outer ring of actuators (38 nm RMS surface with one-third the actuator density of the 8 cm mirror) does not scale sharply with mirror diameter.

Keywords: adaptive optics, carbon fiber, carbon fiber reinforced polymer, CFRP, composite, thin-shell, deformable, adaptive secondary

1. INTRODUCTION

1.1 Science with Deformable Secondary Adaptive Optics Systems

Adaptive Optics systems with deformable secondaries have been in operation since 2002 and many more are planned. The Multiple Mirror Telescope AO system (MMT-AO) with 336 actuator secondary currently delivers Natural Guide Star (NGS) and Ground Layer Laser Guide Star AO (LGS-GLAO). Instrumentation includes BLINC/MIRAC, a thermal infrared (IR) imager; ARIES, a 1-2.5 micron imager and spectrograph; and CLIO, a 3-5 micron imaging camera.¹ Scientific results so far have been predominantly in the thermal infrared, exploiting the uniquely low thermal background of the system.^{2,3,4} Great progress has been made in extrasolar planet searches at thermal IR wavelengths.^{5,6}

The MMT deformable secondary AO system has been used to directly image the three planets orbiting HR8799⁷ at thermal IR wavelengths, finding that the IR colors of the planets do not follow model tracks.⁸ The MMT AO system has also been used to observe Fomalhaut, a star around which a candidate $3M_{\text{Jup}}$ planet was discovered at 96 AU,⁹ taking advantage of the MMT's high contrast in the thermal IR to check for further planets significantly closer to the parent star.¹⁰

*ammons1@llnl.gov; phone 1 925 422-2102; www.u.arizona.edu/~ammons81/

Science with deformable secondary mirrors has been expanding as new instrumentation is built. Deformable secondaries have been constructed for the Large Binocular Telescope (LBT) and the Magellan Telescope¹¹ and are being completed for the Very Large Telescope (VLT).¹² Recent work with one of the Large Binocular Telescope's deformable secondary mirrors has demonstrated the exquisite image sharpness obtainable with these mirrors. The PSFs obtained, with > 80% Strehl in H-band, are among the highest quality images ever taken from the ground at this wavelength.¹³

1.2 Robust, Lightweight Secondary Mirrors for Extremely Large Telescopes

The full D^4 sensitivity of Extremely Large Telescopes (ELTs) is only accessible with adaptive optics working at the diffraction limit of the aperture. Adaptive optics systems for ELTs that use deformable secondary mirrors as the corrective element see even further sensitivity gains over systems that use internal deformable mirrors: They have fewer warm optics, greater total throughput, and thus the higher sensitivity in the mid-IR.¹⁴

The reflective surface of deformable secondaries is constructed with a thin-shell glass membrane, typically of order 1-2 mm thickness for maximum deflection.¹⁵ These thin shells can benefit substantially from the use of robust substrates that are resistant to shattering. In addition, substrates with a lower weight-to-stiffness ratio can reduce the cost of the mounting structure and voice coils by both (1) lowering the mass of the shell and (2) decreasing the force required to deform the shell.

Both the Giant Magellan Telescope (GMT) and the European Extremely Large Telescope (E-ELT) will use deformable secondary mirrors for some AO correction. The secondary mirror of the Giant Magellan Telescope (GMT) comprises seven separate segments, six of which have the same optical figure.¹⁶ With heavy reliance on thin shell deformable secondaries likely to come in the next decade, it will be important that this mode of instrumentation be robust and durable.

1.3 Carbon Fiber Reinforced Polymer as a Deformable Mirror Substrate

Carbon fiber reinforced polymer (CFRP) has been proposed as a robust, lightweight substrate for deformable secondaries.^{17,18} CFRP is a suitable material for optical fabrication because of its low weight-to-stiffness ratio (five times less than steel), a coefficient of thermal expansion (CTE) that can be tuned to near-zero with specialized carbon layup arrangements, and excellent thermal conductivity.¹⁹

Key developments in CFRP technology have enabled its use as a substrate for reflective optics. The ability to tune the in-plane CTE to near-zero is critical for the thermal stability of optical elements. Replicated CFRP mirrors are now free of fiber and core print-through issues and demonstrate sufficient quality of adhesion between coatings and the polymer surface.¹⁹

Figure 1 displays an example manufacturing process for CFRP mirrors (Composite Mirror Applications, CMA, Tucson, AZ). A glass mandrel with the reverse of the desired shape is first polished. Second, strips of CFRP pre-impregnated carbon fiber are layered onto the optical mandrel. The lay-up structure is then cured and released. Upon removal, the quality of the CFRP surface is limited only by the optical figure quality of the mandrel optic.¹⁹ Finally, the optical surface is coated with aluminum using standard techniques for glass mirrors.

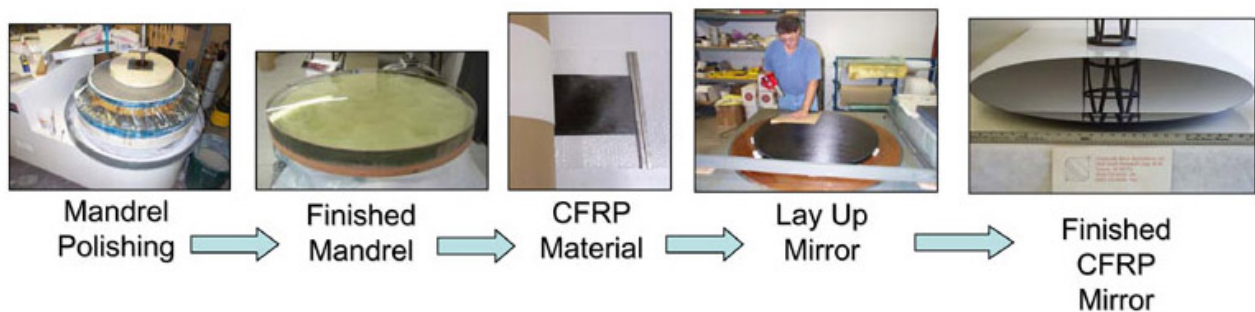


Figure 1. Manufacturing process for CFRP mirrors (from Coughenour et al. 2010; Composite Mirror Applications).

Three principal advantages of using CFRP as a substrate for thin-shell deformable secondaries are as follows:

- (1) *Inherent robustness.* CFRP thin shells are less likely to break under shock than glass during testing, transportation, and installation.
- (2) *Replicability.* Many copies of a single mandrel optic can be made with minimum construction of new components. The mandrel, pressing tools, and other fixtures are only fabricated once.
- (3) *Less actuator force is required.* The curvature of a thin plate induced by a point load is inversely proportional to the thickness of the material cubed.¹⁷ Since CFRP and Zerodur glass have similar Young's moduli and CFRP is resistant to shattering, the thickness of a composite shell can be drastically reduced for substantial savings in the force required to induce a given stroke. For example, a 0.8-mm thick CFRP shell would require nearly 10x less actuator force than a 2-mm thick Zerodur shell, resulting in substantial cost and weight savings in the actuators, internal support structure, and the spider vanes that support the entire assembly.

1.4 Goals of this Paper

To be useful in adaptive optics for infrared astronomy, CFRP deformable secondaries must display good optical figure quality for the ranges of temperature and humidity characteristic of mountaintop observatories. In this paper, we present optical figure tests for two CFRP prototype thin-shell deformable mirrors of different diameters (8 cm and 17 cm). Section 2 discusses the mirror fabrication and the actuator assemblies. In section 3, we review figure quality measurements at a variety of temperatures as well as surface roughness tests for the 8 cm mirror, some of which is previously shown in Coughenour et al. (2010).¹⁷ We also present new interferometric measurements of surface phase at room temperature for the 17 cm piece. Section 4 summarizes the measurements and concludes.

2. 8 CM AND 17 CM THIN SHELL DEFORMABLE MIRRORS

2.1 8 cm Prototype Mirror

Experiments with small CFRP thin-shell mirrors, described below, indicate that their optical figure is sufficient for near-infrared astronomy at a range of temperatures.¹⁷ We have constructed an 8 cm diameter thin-shell CFRP deformable mirror with 1.6 mm substrate thickness (Figure 2, right panel). The surface is concave and spherical. This mirror has seven position actuators mounted to the rear to permit figure testing.

The 8 cm CFRP thin shell mirror is fabricated by Composite Mirror Applications, Inc. (Tucson, AZ) as described in Section 1.3. The mandrel optic is an 80 mm BK7 spherical plano-convex lens with $\lambda/4$ surface figure error. Seven New Focus picomotors are used as position actuators (Figure 2, left panel). The metal tips of the picomotor actuators are forced against the mirror with seven neodymium magnets glued to the rear surface in a hexagonal pattern. Thin, 0.5 mm

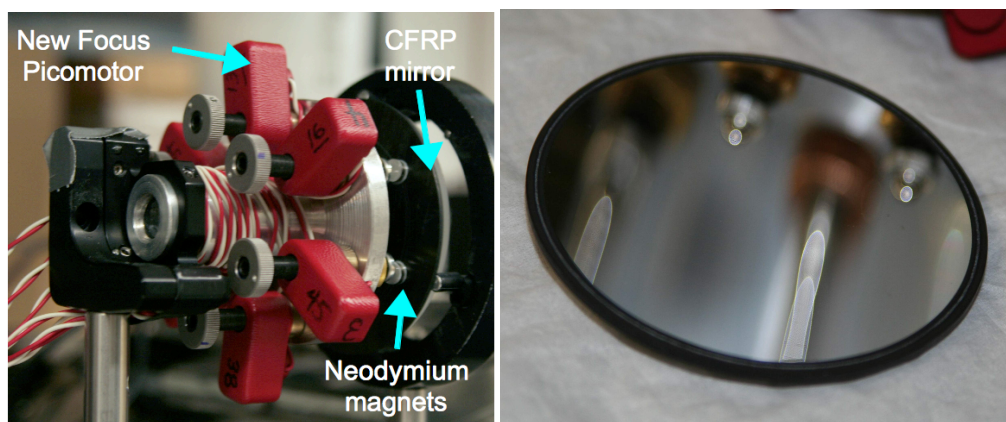


Figure 2: *Left panel:* Mounting apparatus for 8 cm thin shell CFRP mirror. Six New Focus picomotor position actuators are used to control the figure. The central actuator is not automated. *Right panel:* 8 cm spherical CFRP mirror (from Coughenour et al. 2010).

sapphire windows are inserted between the picomotor tips and the magnets to create a smooth surface for position actuation. The gluing technique involves large, single drops of glue (i.e., “single-drop” gluing technique, which produces some surface print-through error at low temperatures). The picomotor actuators are mounted with an aluminum plate, which is kinematically mounted to an optical table. Picomotors are manually, individually actuated with a New Focus driver and control paddle.

2.2 17 cm Prototype Mirror

A 17 cm CFRP prototype thin-shell deformable mirror has been manufactured by CMA for comparison with the 8 cm piece (Figure 3). The layup structure and schedule, carbon fiber material, and material thickness (1.6 mm) are identical to the 8 cm mirror. The 17 cm mirror is manufactured from a 17 cm parabolic lens with a radius of curvature of 680 mm. Nineteen New Focus picomotor position actuators are available to deform the surface. Ten of these actuators are used for the experiments described in Section 3.3. Six of these are in an outer ring of ~14 cm diameter, three are in a smaller ring of ~7 cm diameter, and one is centered. The tips of the picomotors are physically constrained to mirror’s rear surface with neodymium magnets and 0.5-mm thick sapphire windows, as for the 8 cm mirror. Improved gluing techniques are used to reduce gluing stresses (i.e., a “multiple drop” technique is used, in which 3 small, separated drops of glue are deposited in between the sapphire windows, magnets, and CFRP surface).

3. OPTICAL FIGURE RESULTS

3.1 Testing Methodology

Optical figure measurements are performed with a Twyman-Green 4D interferometer (PhaseCam 4020, see Figure 4). For the spherical 8 cm mirror, the distance between the optic and interferometer is set to minimize curvature error. The 4D measurement technique is not sensitive to absolute curvature error, although relative curvature error can be seen as temperature changes. The detailed alignment procedure is described in previous publications.¹⁷

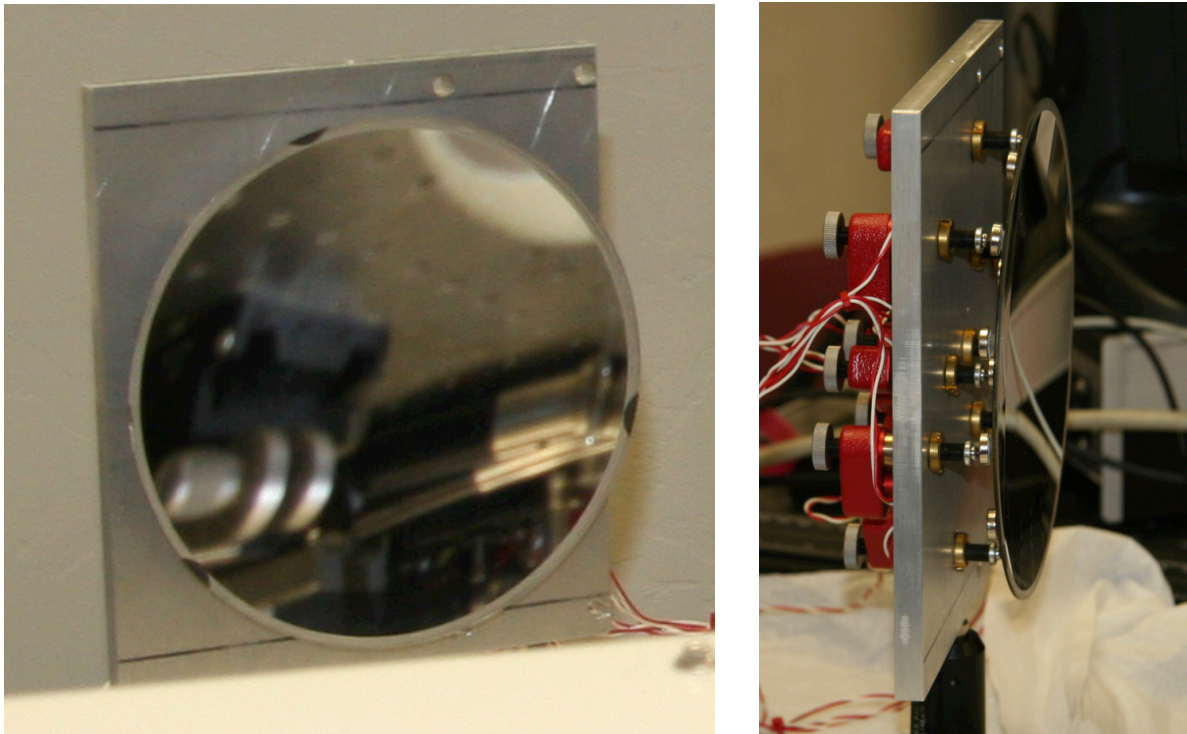


Figure 3. (*left panel*) Front view of 17 cm CFRP parabolic deformable mirror. Picomotor position actuators on the reverse mount the mirror to an aluminum block, which is kinematically mounted to the optical table. (*right panel*) Side view of 17 cm CFRP parabolic deformable mirror. Metal picomotor tips are physically connected to the rear of the mirror with neodymium magnets.



Figure 4: Experimental setup for testing optical figure of CFRP mirrors below 20°C.

Temperature changes are induced by testing a mirror in a commercial freezer (Figure 4) capable of reducing the temperature to -20°C . The mirror under test is not in contact with the freezer and is kinematically mounted to the optical breadboard underneath. The interferometer laser is directed through a hole in the freezer. A glass membrane is placed at the hole to prevent thermal cycling with the uncontrolled environment, which induces a negligible amount of spherical aberration in the test beam (~ 20 nm RMS for both mirrors) and much less astigmatism and coma error. A desiccant is kept in the chamber to keep the interior dry and the mirror defogged at low temperatures.

The test setup for the 17 cm parabolic mirror is similar to that of the spherical 8 cm mirror. The principal on-axis difference between a spherical figure and a parabolic figure is spherical aberration, which is removed in software. The mirror is first aligned with only three actuators connected to the mirror. The tip/tilt and piston of the mirror and the tip/tilt of the incoming beam are then iteratively adjusted to remove curvature, astigmatism, and coma errors, all of which can be introduced when the optical axis of the mirror is misaligned with the test beam. Once these Zernike coefficients are minimized, the expected difference between the parabolic shape and a spherical mirror of equivalent radius of curvature is removed in software. The figure of this difference is entirely spherical aberration. Note that this procedure is blind to absolute curvature, astigmatism, and coma, although relative changes in these modes can be measured as temperature or humidity changes.

For the 17 cm mirror, the rectangular entrance hole to the freezer vignettes the beam by ~ 2.0 cm on the left and right sides. We characterize the figure in a 13 cm by 17 cm section that represents 87% of the reflective area of the mirror.

3.2 Optical Figure Data for 8 cm Piece

3.2.1. *Fizeau fringe maps.* We have used Fizeau interferometry to estimate the optical quality with and without using the actuators to optimize the figure. The interferometric fringe pattern of the 8 cm piece, when supported by 3 actuators, is an indication of its natural, relaxed figure. We find that this shape is dominated by curvature, as expected. The print-through errors are ~ 100 nm P-V on the surface. The remaining wavefront error across the piece is less than 150 nm RMS wavefront (< 75 nm RMS surface). Figure 5 displays the interferometric fringes of the 8 cm piece under the best manual actuator correction at room temperature. The error is less than 80 nm RMS wavefront (< 40 nm RMS surface) across the

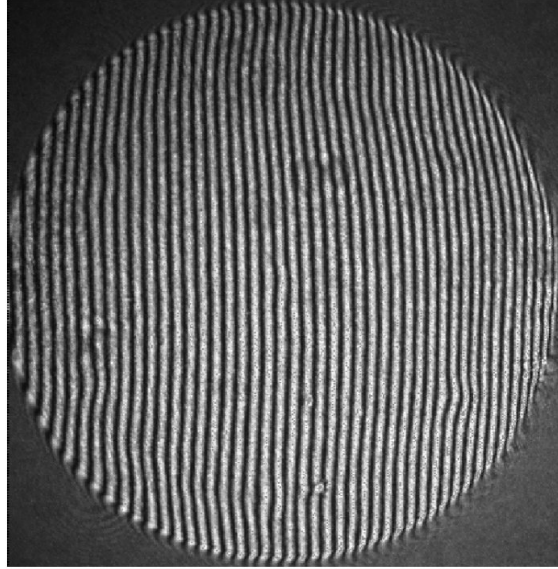


Figure 5: Fizeau interferometer fringes of 8 cm mirror under best 6-actuator correction at 20°C (from Coughenour et al. 2010).

entire mirror. Computer-controlled optimization of actuator commands may improve this performance. Most of the error appears to be edge curvature, beyond the correctable radius of the actuators. The forces required to correct the natural, relaxed shape of the 8 cm CFRP piece are estimated to be ~ 0.1 N for each actuator.¹⁷ These values are well within the dynamic range of voice coils (1-2 N), which are commonly used as deformable secondary actuators.

3.2.2 Surface Roughness. We have used a Veeco white light interferometer to scan small, $116 \times 155 \mu\text{m}$ patches of the surface of the mirror at room temperature. A representative patch is displayed in Figure 6. The average measured surface roughness is 3 nm P-V, sufficient for optical and near-infrared wavelengths. White light interferograms using larger patch sizes indicate that the errors on ~ 0.5 mm spatial scales are small (< 10 nm RMS).

3.2.3 Surface Error at Colder Temperatures. Although the CTE of CFRP is near zero, some surface error is expected with temperature variation due to non-zero CTE out of plane. We have tested the optical figure of the 8 cm mirror at a variety of temperatures to constrain this effect. Figure 7 displays the mirror fringes at -5°C under the best manual actuator correction. Notice that the error is dominated by uncorrectable edge curvature, which will be negligible for larger mirrors. Near room temperature, the RMS error internal to the outer ring of actuators is quite small (17 nm RMS surface). Decreasing the temperature increases this error to 40 nm RMS at -5°C .¹⁷ Optimizing the actuator positions at lower temperatures improves the figure error to 33 nm RMS at -5°C .

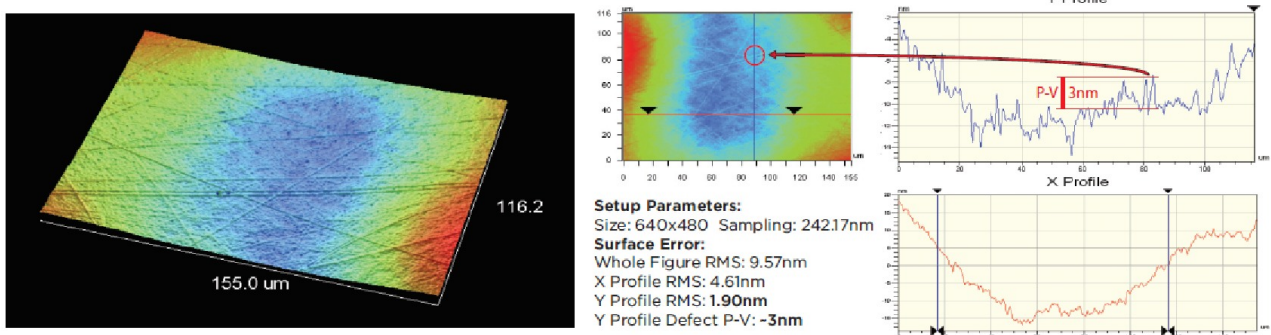


Figure 6: Veeco white light interferogram of a $116 \times 155 \mu\text{m}$ patch of the 8 cm CFRP mirror at 20°C. The left and middle panels display the phase as color. Individual carbon fibers are seen in the phase map. The right panels display horizontal and vertical cuts of the phase. The overall curvature seen in the phase map is due to the prescribed spherical curvature of the mirror. The surface roughness of the piece due to the carbon fibers is 3 nm P-V (from Coughenour et al. 2010).



Figure 7: Interferometric fringes of 8 cm piece under best 6-actuator correction at -5°C . “Single-drop” gluing techniques for the actuator magnets produce gluing stress errors of up to 0.6 microns P-V. These errors are not seen in the 17 cm parabola, which uses “multiple-drop” gluing.

3.3 Preliminary optical figure measurements of 17 cm parabola

Following the optical alignment technique described in Section 3.1., we have used a 4-D interferometer to characterize the optical figure of the 17 cm parabola under the best manual 10-actuator correction at room temperature. The phase map is shown in Figure 8. The overall surface error is 138 nm RMS. The surface error with all Zernike modes up to fifth order removed is 53 nm RMS. The component of this high-order error internal to the outer ring of actuators, which avoid uncorrectable high-order edge curvature, is 38 nm RMS surface.

Note that the dominant error is tricoma, which is currently an uncorrectable mode with only 6 actuators in the outer ring. Uncorrectable edge curvature beyond the outer ring of actuators is also a significant component. The surface error should decrease when all 19 actuators are used for correction and when the flattening is computer controlled. Note that the actuator density of the 17 cm piece (0.044 actuators per cm^2 with 10 active picomotors) is less than one-third of that of the 8 cm piece (0.139 actuators per cm^2), so more intra-actuator error is expected for the larger mirror.

4. DISCUSSION

We have characterized the surface figure error of an 8 cm CFRP thin-shell deformable mirror over the temperature range characteristic of a mountaintop observatory. Similar thermal cycling experiments with a 19-actuator 17-cm CFRP parabola are ongoing.

The optical figure experiments of the 8 cm spherical prototype indicate that:

- The natural, relaxed optical figure is close (< 75 nm surface) to the prescribed figure. Relaxation of CFRP's internal stresses produces tolerable deformations. These low-amplitude deformations are dominated by curvature.
- The optical figure under the best qualitative actuator correction (< 40 nm RMS surface) places it into consideration for use in near-IR astronomy. The contribution of this error term alone only reduces K-band Strehl to 95%.
- Actuator print-through is small at room temperature (~ 100 nm P-V surf.).

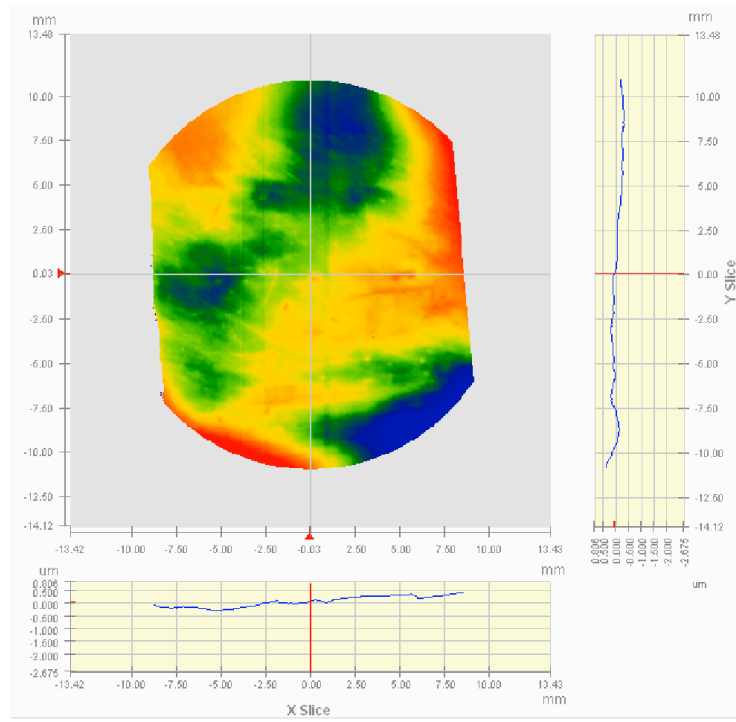


Fig. 8. Optical figure map of 17 cm CFRP parabolic deformable mirror at 20°C. The phase is presented over a 13 cm by 17 cm section of the mirror (87% of the full illuminated aperture). Horizontal and vertical cuts through the phase are shown to the side and below. The optical error is 138 nm RMS surface over the illuminated aperture and 53 nm RMS surface with all low-order modes up to fifth radial order removed. Piston, tip/tilt, focus, and astigmatism modes have been removed. The entrance hole to the environmental chamber vignettes the full beam on the left and right, necessitating the vertical rectangular aperture. Ten actuators in three concentric rings have been used to correct for some low-order figure error.

- The actuator forces required to correct the figure (~ 0.1 N) are small compared to the dynamic range of voice coil actuators.
- The error internal to the outer ring of actuators, which is representative of what the figure error of a larger mirror would be under an optimal actuator correction, remains low (< 35 nm RMS surface) over the temperature range investigated (-5°C - 20°C).
- Surface roughness is low at room temperature (~ 3 nm P-V).

Preliminary figure experiments with the 17 cm parabola under manual 10-actuator correction give 138 nm RMS surface error over a 13 cm x 17 cm section of the mirror. The uncorrectable high-order component of this error internal to the outer ring of actuators (“intra-actuator” error) is 38 nm RMS surface. For comparison, the intra-actuator error of the 8 cm piece is 17 nm RMS with higher actuator density (0.14 actuators per cm^2 as compared to 0.044 actuators per square cm^2 for the 17 cm piece). The intra-actuator error of these CFRP mirrors does appear to scale with mirror diameter, but not sharply. The difference is likely due to the factor of 3 difference in actuator density. The figure error of the 17 cm piece is expected to decrease when all 19 actuators are used and when the flattening is optimized by computer.

5. ACKNOWLEDGEMENTS

Thanks to Michael Tuell of the University of Arizona Mirror Laboratory for loan of a Twyman-Green 4D interferometer to support these experiments. SMA recognizes support from the Space Telescope Science Institute through the Hubble Postdoctoral Fellowship and the LLNL Lawrence Postdoctoral Fellowship.

This work performed under the auspices of the U.S. Department of Energy by Lawrence Livermore National Laboratory under Contract DE-AC52-07NA27344.

REFERENCES

- [1] Freed, M., Hinz, P., Meyer, M., Milton, N.M., and Lloyd-Hart, M., "Clio: a 5 micron camera for the detection of giant exoplanets," in *Groundbased Instrumentation for Astronomy*, Proc. SPIE, 5492, 1561 (2004).
- [2] Close, L., Wildi, F., Lloyd-Hart, M., et al., "High resolution images of orbital motion in the Trapezium cluster: first scientific results from the MMT deformable secondary mirror adaptive optics system," *ApJ*, 599, 537 (2003).
- [3] Close, L., Biller, B., Hoffmann, W.F., et al., "Mid-infrared imaging of the post-AGB star AC Herculis with the MMT adaptive optics system," *ApJL*, 598, L35 (2003).
- [4] Biller, B. A., Close, L. M., Li, A., Biegging, J. H., Hoffmann, W. F., Hinz, P. M., Miller, D., Brusa, G., Lloyd-Hart, M., Wildi, F., Potter, D., and Oppenheimer, B., "High resolution midinfrared imaging of the AGB star RV Boo with the Steward Observatory adaptive optics system," *ApJ*, 620, 450 (2005).
- [5] Nielsen, E. and Close, L., "A Uniform Analysis of 118 Stars with High-Contrast Imaging: Long Period Extrasolar Giant Planets are Rare around Sun-like Stars," *ApJ*, 717, 878 (2010).
- [6] Biller, B.A., Close, L., Masciadri, E., et al., "An Imaging Survey for Extrasolar Planets around 45 Close, Young Stars with the Simultaneous Differential Imager at the Very Large Telescope and MMT," *ApJS*, 173, 143 (2007).
- [7] Marois, C., Macintosh, B., Barman, T. et al., "Direct Imaging of Multiple Planets Orbiting the Star HR 8799," *Science*, 322, 1348 (2008).
- [8] Hinz, P., et al., "Thermal Infrared MMTAO Observations of the HR 8799 Planetary System," *ApJ*, 716, 417 (2010).
- [9] Kalas, P., Graham, J., Chiang, E., et al., "Optical Images of an Exosolar Planet 25 Light-Years from Earth," *Science*, 322, 1345 (2008).
- [10] Kenworthy, M.A., Mamajek, E., Hinz, P., et al., "MMT/AO 5 μm Imaging Constraints on the Existence of Giant Planets Orbiting Fomalhaut at $\sim 13\text{-}40$ AU", *ApJ*, 697, 1928 (2009).
- [11] Close, L., Gasho, V., Kopon, D., et al., "The Magellan Telescope Adaptive Secondary AO System," *proc. SPIE*, 7015, 0 (2009).
- [12] Arsenault, R., Madec, P.-Y., Hubin, N., et al., "ESO adaptive optics facility," *proc. SPIE*, 7015, 24 (2008).
- [13] Esposito, S., et al., "First light AO (FLAO) system for LBT: final integration, acceptance test in Europe, and preliminary on-sky commissioning results," *proc. SPIE*, 7736, 7 (2010).
- [14] Lloyd-Hart, M., "Thermal Performance Enhancement of Adaptive Optics by Use of a Deformable Secondary Mirror," *PASP*, 112, 264 (2000).
- [15] Brusa, G., Riccardi, A., Salinari, P., et al., "MMT adaptive secondary: performance evaluation and field testing", *proc. SPIE*, 4839, 691 (2003).
- [16] Hinz, P., et al., "The GMT Adaptive Optics System," *proc. SPIE*, 7736, 10 (2010).
- [17] Coughenour, B., Ammons, S.M., Hart, M., et al., "Demonstration of a Robust Curved Carbon Fiber Reinforced Polymer Deformable Mirror with Low Surface Error," *proc. SPIE*, 7736, 117 (2010).
- [18] Kendrew, S. and Doel, P., "Finite element analysis of carbon fiber composite adaptive mirrors," *proc. SPIE*, 5490, 1591 (2004).

[19] Romeo, R. and Martin, R., "Progress in 1m-class lightweight CFRP composite mirrors for the ULTRA telescope," Proc. SPIE 6273, 62730 (2006).